

Biomass-Derived Single Zn Atom Catalysts: The Multiple Roles of Single Zn Atoms in the Oxidative Cleavage of C–N Bonds

Jingzhong Qin, Bo Han, Xiaomei Lu, Jiabao Nie, Chensheng Xian, and Zehui Zhang*



Cite This: *JACS Au* 2023, 3, 801–812



Read Online

ACCESS |



Metrics & More



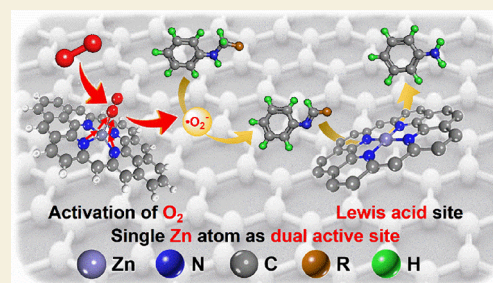
Article Recommendations



Supporting Information

ABSTRACT: The C–N bond cleavage represents one kind of important organic and biochemical transformation, which has attracted great interest in recent years. The oxidative cleavage of C–N bonds in *N,N*-dialkylamines into *N*-alkylamines has been well documented, but it is challenging in the further oxidative cleavage of C–N bonds in *N*-alkylamines into primary amines due to the thermally unfavorable release of α -position H from N–C $_{\alpha}$ –H and the paralleling side reactions. Herein, a biomass-derived single Zn atom catalyst (ZnN₄-SAC) was discovered to be a robust heterogeneous non-noble catalyst for the oxidative cleavage of C–N bonds in *N*-alkylamines with O₂ molecules. Experimental results and DFT calculation revealed that ZnN₄-SAC not only activates O₂ to generate superoxide radicals ($\cdot\text{O}_2^-$) for the oxidation of *N*-alkylamines to generate imine intermediates (C=N), but the single Zn atoms also served as the Lewis acid sites to promote the cleavage of C=N bonds in imine intermediates, including the first addition of H₂O to generate α -hydroxylamine intermediates and the following C–N bond cleavage via a H atom transfer process.

KEYWORDS: single Zn atom, cleavage of C–N bonds, Lewis acid sites, superoxide radical ($\cdot\text{O}_2^-$), amines, nitriles



INTRODUCTION

Amines are one of the most important building blocks in organic chemistry.¹ They are widespread in the core structure of high-value materials like drugs and agrochemicals.^{2,3} The oxidative functionalization of C–N bonds by bio-enzymes plays a vital role in nature from both transformative and drug metabolism aspects.⁴ Among different types of oxidative functionalizations of C–N bonds, the oxidative cleavage of C–N bonds (also called N-dealkylation) in *N,N*-dialkylamines (tertiary amines) or *N*-alkylamines (secondary amines) represents an important type of biochemical reaction and chemical transformation, particularly in the pharmaceutical industry.^{5–8}

From the viewpoints of green and sustainable chemistry, the use of O₂ as the terminal oxidants for the oxidative cleavage of C–N bonds in *N,N*-dialkylamines or *N*-alkylamines represents an environmentally friendly and economical methodology.⁹ The oxidative cleavage of C–N bonds in *N,N*-dialkylamines into *N*-alkylamines has been well documented over noble or non-noble metal catalysts.^{10,11} However, the further oxidative cleavage of C–N bonds in *N*-alkylamines into primary amines remains a challenging target, and it has been rarely reported. As shown in Figure 1a, one of the great challenges in the oxidative cleavage of C–N bonds in *N*-alkylamines is the presence of three well-known competitive reactions, namely, the direct N-oxidation to give *N*-oxides,¹² the carbonylation of the α -carbon to generate amides,^{13–15} and the oxidation of the C(sp³)–C(sp³) bond to produce enamines.¹⁶ Being more challenging,

the release of α -position H from N–C $_{\alpha}$ –H in *N*-alkylamines was thermally unfavorable by the thermal-catalytic approaches, which was the crucial step in the oxidative cleavage of C–N bonds in *N*-alkylamines into primary amines.¹⁷

To the best of our knowledge, only one photochemical approach is enlightened for the oxidative cleavage of C–N bonds in *N*-alkylamines into primary amines by the binary homogeneous catalysts of Ir complexes and Co complexes with Et₃N as the base additive (Figure 1b), which was based on the light-irradiated single-electron transfer (SET) strategy.¹⁸ Obviously, this method suffered from distinct disadvantages in terms of the use of high-cost Ir complexes and the difficulty in the recycle of combined Ir and Co complexes. In current catalytic systems, the design of heterogeneous non-noble metal catalysts for chemical reactions is highly demanded because of the low catalyst cost and the facile recycle of the catalyst and the purification of aim products. However, there exists no such heterogeneous non-noble catalytic system for the oxidative cleavage of C–N bonds in *N*-alkylamines into primary amines.

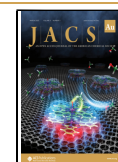
In recent years, single metal atom catalysts (SACs) have received particular interest in electron chemistry and chemical

Received: November 7, 2022

Revised: January 1, 2023

Accepted: January 4, 2023

Published: February 16, 2023



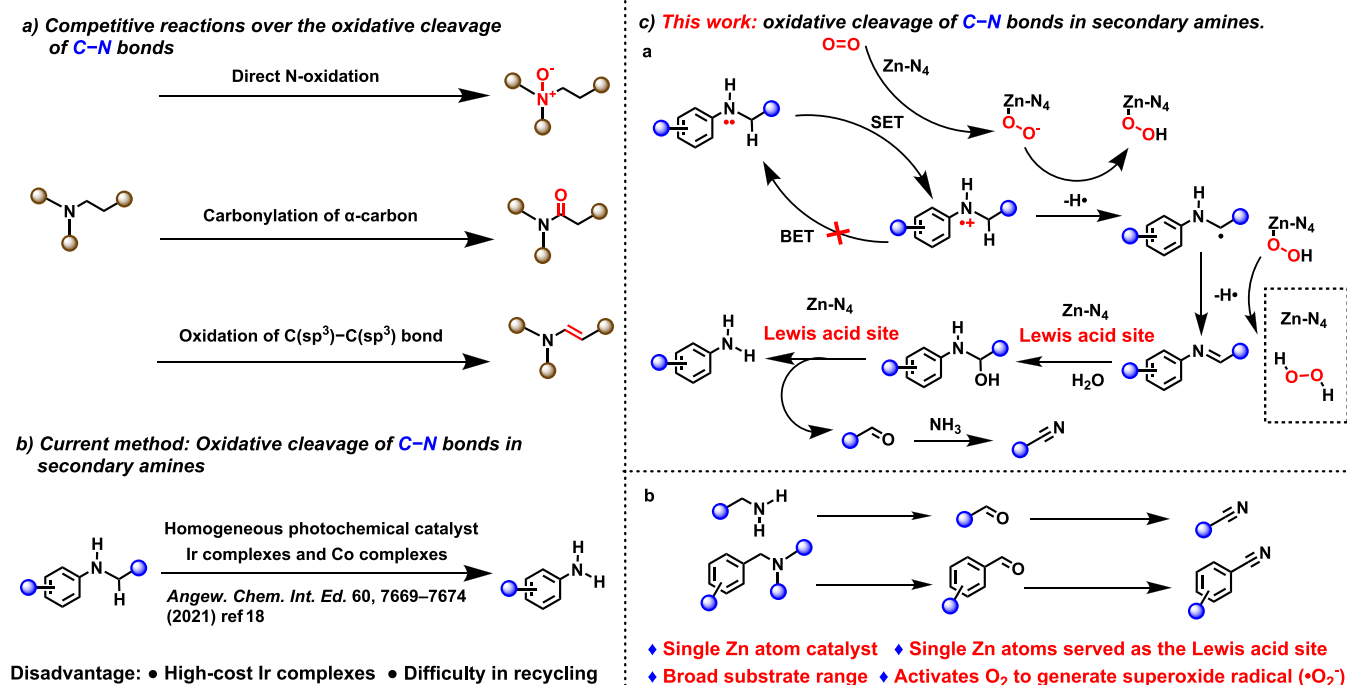


Figure 1. Methods of the oxidative cleavage of C–N bonds in *N*-alkylamines. (a) Competitive reactions over the oxidative cleavage of C–N bonds. (b) Current method. (c) This work.

reactions^{19–21} because of the full atomic utilization and some unique properties of single metal atoms. Some single metal atom catalysts demonstrated good catalytic performance for some oxidation reactions such as the aerobic oxidation of alcohols, carbon monoxide, and methane.^{22–24} In addition, the single metal atoms can also serve as Lewis acid sites to activate some substrates to improve the catalytic efficiency.²⁵ For example, Jiang and co-workers prepared nitrogen-coordinated single Zn atoms from polystyrene (PS) nanosphere-modified Zn-MOF, and they achieved high catalytic efficiency of the CO₂ cycloaddition with epoxides, where the single Zn and N atoms served as the Lewis acid site and Lewis base site for the synergistic activation of substrates, respectively.²⁵ To achieve the success in the oxidative cleavage of C–N bonds in the challenging *N*-alkylamines, the simultaneous activation of O₂ and the *N*-alkylamine molecules might be an ideal and effective strategy. In this case, the single Zn atom catalyst is anticipated to meet the dual requirements by the activation of O₂ molecules via the electron-transfer process and the activation of *N*-alkylamines by the interaction of N atoms in *N*-alkylamines and single Zn atoms in the catalyst (called as Lewis base–Lewis acid interaction). Herein, the single Zn atom catalyst bearing Zn–N₄ motifs was facilely prepared by the pyrolysis of a biomass-derived lignin alkali-coordinated single Zn complex. As expected, the as-prepared single Zn atom catalyst was discovered to be robust for the oxidative cleavage of C–N bonds in these challenging *N*-alkylamines with O₂ as the terminal oxidant (Figure 1c).

RESULTS AND DISCUSSION

Catalyst Preparation and Characterization

As shown in Figure 2a, the biomass-derived lignin alkali was used as the polymer precursors to host Zn²⁺ via the coordination with nitrogen atoms in lignin alkali. Due to the evaporation of the Zn atoms beyond 908 °C, the pyrolysis

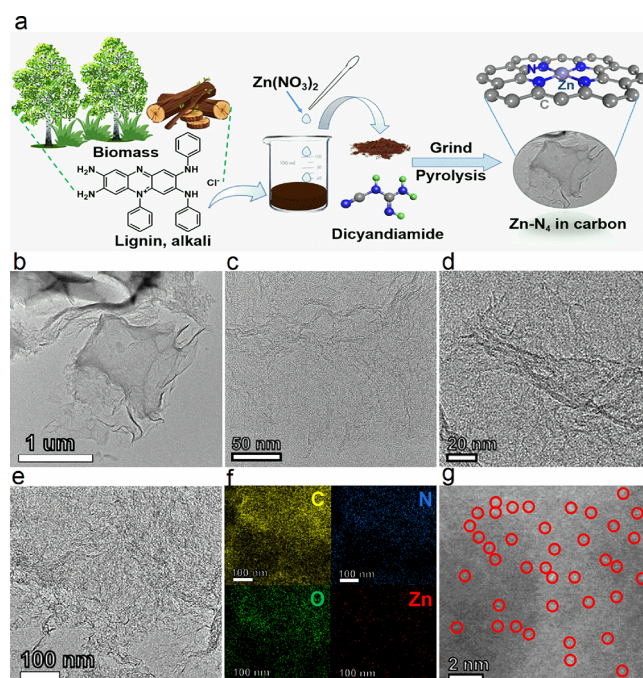


Figure 2. Preparation and characterizations of the ZnN₄-SAC catalyst. (a) Procedure of the preparation of the ZnN₄-SAC catalyst; (b–e) TEM images; (f) corresponding EDS mapping images (C, yellow; N, blue; O, green; Zn, red); and (g) AC-HAADF-STEM image.

temperature was set at 1000 °C to obtain the ZnN₄-SAC catalyst, where each single Zn atom was coordinated by four nitrogen atoms. Pyrolysis of the lignin alkali–Zn complex and dicyandiamide at 1000 °C gave rise to the ZnN₄-SAC catalyst with a Zn weight percentage of 0.67% as determined by ICP-AES (Table S1). ZnN₄-SAC exhibits a large Brunauer–Emmett–Teller (BET) surface area of 584 m²/g and a pore

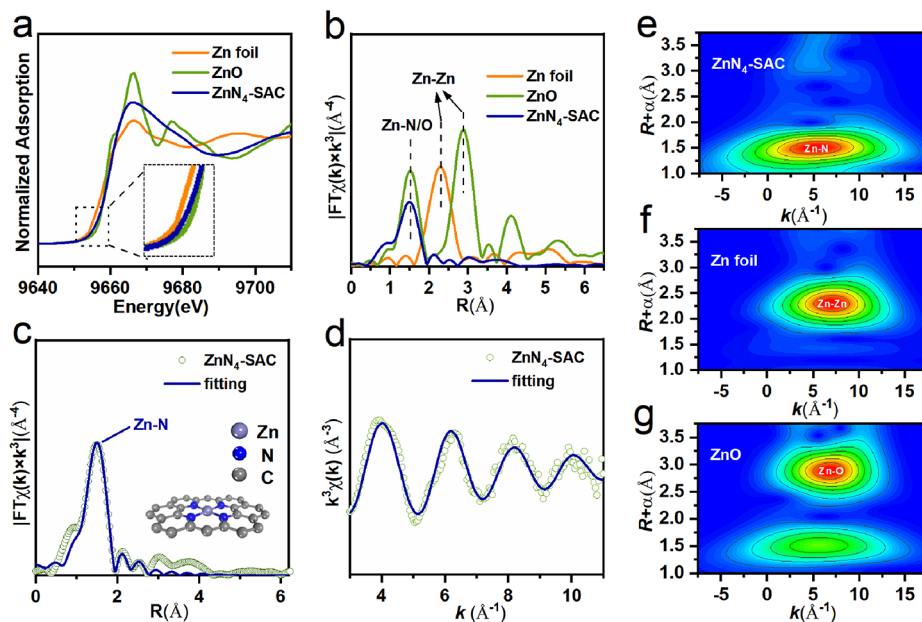


Figure 3. Characterizations of the $\text{ZnN}_4\text{-SAC}$ catalyst. (a) XANES spectra; (b) FT-EXAFS spectra in the R space; fitted FT-EXAFS spectra in the (c) R space and (d) k space (the inset shows the atomic structure model of the Zn–N₄ motif in the $\text{ZnN}_4\text{-SAC}$ catalyst); (e–g) WT-EXAFS plots.

volume of $0.96 \text{ cm}^3/\text{g}$ (Figure S1 and Table S1). Its high surface area should be ascribed to its unique 2D porous nature caused by Zn salt-assisted pyrolysis, where most of the Zn atoms served as the soft template and evaporated off during the pyrolysis process. The large surface area of the $\text{ZnN}_4\text{-SAC}$ catalyst with abundant pores benefits the mass transfer of the reaction/production molecules during the reaction process.²⁶

The X-ray powder diffractometry (XRD) patterns of $\text{ZnN}_4\text{-SAC}$ only show two weak peaks with 2θ at 26.5° and 44.6° (Figure S2), corresponding to the (002) and (101) planes of the graphitic carbon, respectively.²⁷ Raman spectrum (Figure S3) shows two peaks with the center at 1341 and 1591 cm^{-1} , which are associated with the defective carbon (D-band) and sp^2 -hybridized carbon network (G-band), respectively. Transmission electron microscopy (TEM) images of $\text{ZnN}_4\text{-SAC}$ revealed a thin-layer structure without any visible nanoparticles or clusters for Zn species (Figure 2b–e). Energy-dispersive X-ray spectroscopy (EDX) composition analysis (Figure 2f) shows a homogeneous distribution of Zn, N, and O elements on the carbon support of the $\text{ZnN}_4\text{-SAC}$ catalyst. Then, we resorted to the aberration-corrected high-angle annular dark-field scanning transmission electron microscopy (AC-HAADF-STEM) image to identify the Zn species. As shown in Figure 2g, isolated single Zn atoms anchored on a nitrogen-doped carbon layer were clearly identified as the brighter spots, which were circled in red for better observation. Regarding the N 1s XPS spectrum, four types of nitrogen species were fitted as follows (Figure S4): oxidized N (403.1 eV), graphitic N (401.1 eV), Zn–N_x (399.6 eV), and pyridinic N (398.1 eV).²⁸ The calculated percentage contents of oxidized N, graphitic N, Zn–N_x, and pyridinic N species are 4, 31, 12, and 53%, respectively. Clearly, these nitrogen species (oxidized N, graphitic N, and pyridinic N) can serve as anchor sites to stabilize the single Zn atoms.²⁹

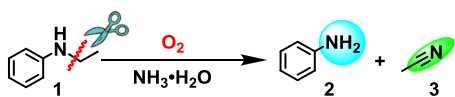
Element-selective X-ray absorption fine structure (XAFS) measurements at the Zn K-edge were performed to investigate the valence state and coordination environment of Zn species. Figure 3a shows the X-ray absorption near-edge structure

(XANES) spectra of $\text{ZnN}_4\text{-SAC}$ along with standard Zn foil and ZnO references. The normalized X-ray absorption near-edge structure curves for the Zn K-edge show that the absorption edge energy of $\text{ZnN}_4\text{-SAC}$ is far from that of Zn foil, but close to that of ZnO, suggesting that the valence state of Zn in $\text{ZnN}_4\text{-SAC}$ should be close to +2. The Fourier transform (FT) k^2 -weighted extended X-ray absorption fine structure (FT-EXAFS) spectrum of $\text{ZnN}_4\text{-SAC}$ (Figure 3b) exhibits only one obvious peak located at 1.45 \AA , which should be attributed to the Zn–N/O contribution.³⁰ No Zn–Zn peaks were observed in the FT-EXAFS spectra of $\text{ZnN}_4\text{-SAC}$, further suggesting that all the single Zn atoms were coordinated with the nitrogen atoms or oxygen atoms without the presence of ZnO and metallic Zn. First-shell FT-EXAFS fitting was performed to extract structural parameters (Figure 3c,d and Table S2). On the basis of the best-fitting results, each single Zn atom was coordinated by four nitrogen atoms in $\text{ZnN}_4\text{-SAC}$. Therefore, the Zn species in the as-prepared catalyst should be present in Zn–N₄ motifs. Additionally, the wavelet transforms (WT) of Zn K-edge EXAFS oscillations are also provided (Figure 3e–g). The contour plots of the $\text{ZnN}_4\text{-SAC}$ catalyst present only one intensity maximum at 5 \AA^{-1} , corresponding to the Zn–N coordination, and no intensity maxima related to Zn–Zn and Zn–O coordination were detected by comparison with Zn foil and ZnO references.

Catalyst Screening and Optimizing the Reaction Conditions

As we stated above, the oxidative cleavage of C–N bonds in *N*-alkylamines into primary amines is rather challenging. To our great pleasure, the $\text{ZnN}_4\text{-SAC}$ catalyst demonstrated good catalytic performance for the oxidative cleavage of C–N bonds in *N*-ethylbenzylamine, affording a conversion of 56% and a high aniline selectivity of 93% at 150°C within 4 h (Table 1, entry 1). The benchmark reaction delivered no conversion over nitrogen-doped carbon (NC-1000), suggesting that the single Zn atoms in the $\text{ZnN}_4\text{-SAC}$ catalyst were crucial for the oxidative cleavage of C–N bonds in *N*-ethylbenzylamine (Table 1, entry 2). As the biomass-derived lignin alkali may

Table 1. Catalyst Screening of the Oxidative Cleavage of C–N Bonds in *N*-Ethylaniline^a



| entry | catalyst | temperature (°C) | conversion of 1 (%) | selectivity of 2 (%) |
|----------------|----------------------------|------------------|---------------------|----------------------|
| 1 | ZnN ₄ -SAC | 150 | 56 | 93 |
| 2 | NC-1000 | 150 | 0 | |
| 3 ^b | ZnN ₄ -SAC | 150 | 15 | 93 |
| 4 | Zn–N _x /NC-1100 | 150 | 20 | 95 |
| 5 | ZnPc | 150 | 0 | |
| 6 | Cu ₂ | 150 | 0 | |
| 7 | Cu(OAc) ₂ | 150 | 0 | |
| 8 | FeCl ₃ | 150 | 0 | |
| 9 ^c | ZnN ₄ -SAC | 150 | 32 | 37 |

^aReaction conditions: *N*-ethylaniline (0.4 mmol), catalyst (40 mg), 1,4-dioxane (4 mL), NH₃·H₂O (26.5 wt %, 400 μL), O₂ (10 bar), 150 °C, and 4 h. ^b1 mmol of KSCN was added. ^cThe reaction was performed without NH₃·H₂O.

contain other impurity metal ions (e.g., Mn, Fe, Cu, etc.) contributing to the catalytic activity, the concentration of metal ions in NC-1000 and ZnN₄-SAC catalyst solution (fully dissolved) was investigated with ICP-AES (Table S3). As shown in Table S3, the controlled experiments revealed that no other metals are present in the starting materials for the preparation of the single Zn catalysts. The above results indicate that Zn is crucial in this reaction. The poisoning experiment by KSCN greatly inhibited the catalytic activity of ZnN₄-SAC (Table 1, entry 3) because of the strong affinity of SCN[−] to single Zn atoms.³¹ The poisoning experiment further confirmed that the Zn–N_x motifs were active sites. In addition, the Zn–N_x/NC-1100 catalyst was also prepared by the same procedures as those for the ZnN₄-SAC catalyst, but the pyrolysis temperature was set to 1100 °C. Preliminary characterizations (Figures S1–S5) revealed that the Zn species should also be present as single Zn atoms. Compared with the ZnN₄-SAC catalyst, the Zn–N_x/NC-1100 catalyst with the same catalyst loading demonstrated a much lower conversion (Table 1, entries 1 vs 4) due to its much lower Zn content (0.07 wt %, Table S1). Furthermore, the catalytic performance

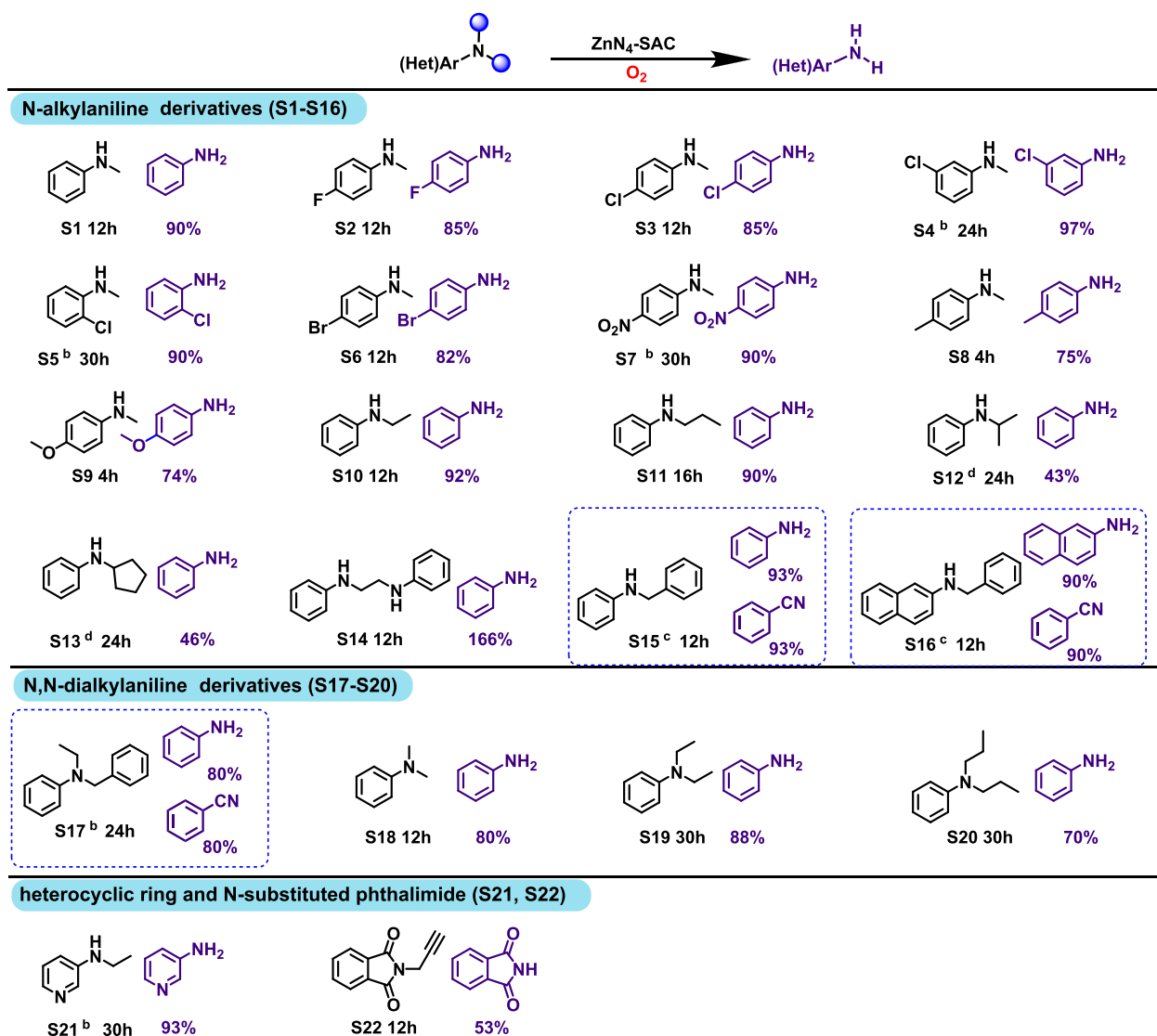


Figure 4. Oxidative cleavage of C–N bonds in *N*-alkylanilines and *N,N*-dialkylanilines. Reaction conditions: substrate (0.4 mmol), ZnN₄-SAC (40 mg), NH₃·H₂O (26.5 wt.% 400 μL), 1,4-dioxane (4 mL), O₂ (10 bar), 150 °C. Superscript b: 160 °C. Superscript c: 120 °C. Superscript d: 180 °C.

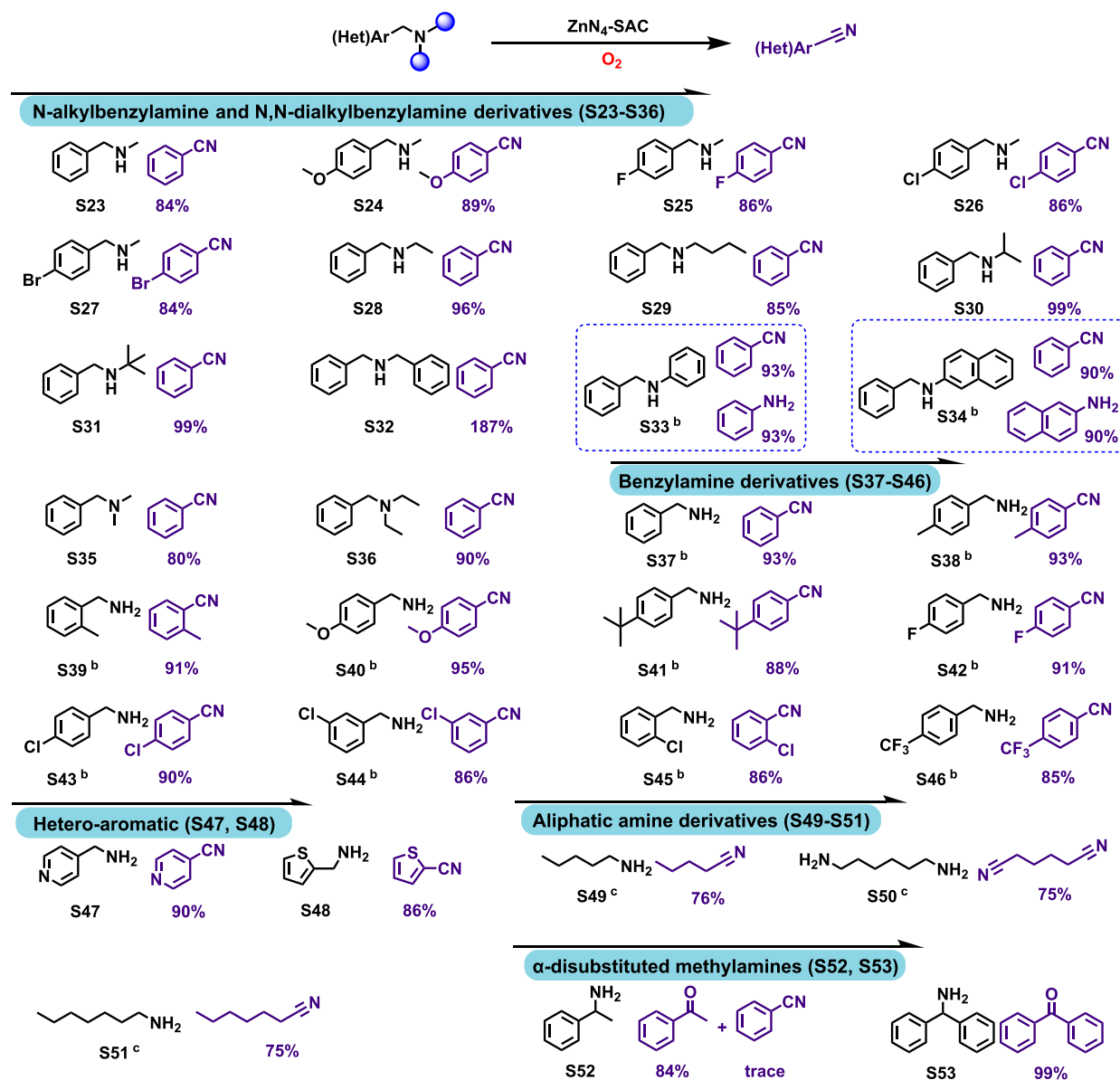


Figure 5. Oxidative cleavage of C–N bonds in *N*-alkylbenzylamines, *N,N*-dialkylbenzylamines, and benzylamine derivatives. Reaction conditions: substrate (0.4 mmol), $\text{ZnN}_4\text{-SAC}$ (40 mg), $\text{NH}_3\cdot\text{H}_2\text{O}$ (26.5 wt % 400 μL), 1,4-dioxane (4 mL), O_2 (10 bar), 150 $^\circ\text{C}$, and 12 h. Superscript b: 120 $^\circ\text{C}$ and 12 h. Superscript c: 70 $^\circ\text{C}$ and 20 h.

of the $\text{ZnN}_4\text{-SAC}$ catalyst was also superior to other homogeneous transition metal catalysts. Homogeneous ZnPc showed no catalytic activity for the oxidative transformation of *N*-ethylaniline into aniline (Table 1, entry 5). The Cu and Fe salts, which were reported active in activating O_2 ,^{32,33} were also unable to catalyze this transformation (Table 1, entries 6–8).

Then, the reaction conditions were optimized for the oxidative cleavage of C–N bonds in *N*-ethylbenzylamine over the $\text{ZnN}_4\text{-SAC}$ catalyst. The reaction solvents showed a great influence on this transformation (Table S4). Better catalytic performance was observed in polar solvents due to their strong ability to disperse the $\text{ZnN}_4\text{-SAC}$ catalyst and dissolve the substrates and the $\text{NH}_3\cdot\text{H}_2\text{O}$. 1,4-Dioxane was screened to be the best reaction solvent. The oxygen pressure was positive from 2.5 to 10 bar toward this transformation (Table S5) because the increase in the O_2 pressure resulted in the increase in oxygen concentration in the reaction solvent and on the catalyst surface. In addition, the $\text{NH}_3\cdot\text{H}_2\text{O}$ additive was found

to be important for the oxidative transformation of *N*-ethylaniline into aniline (Table 1, entries 1 vs 9). The *N*-ethylaniline conversion decreased greatly from 56 to 32% without $\text{NH}_3\cdot\text{H}_2\text{O}$. More importantly, the aniline selectivity decreased greatly from 93 to 37%. To explain the significance of $\text{NH}_3\cdot\text{H}_2\text{O}$, we performed relevant controlled experiments with *N*-benzylideneaniline as a substrate in the absence of $\text{NH}_3\cdot\text{H}_2\text{O}$ (Figure S6a). The results showed that *N*-benzylideneaniline, aniline, and benzaldehyde achieved equilibrium after 8 h, leaving the conversion remaining at 68% after another 6 h. However, with *N*-benzylideneaniline as a substrate in the presence of $\text{NH}_3\cdot\text{H}_2\text{O}$ (Figure S6b), benzaldehyde was further converted to benzonitrile, thereby consuming benzaldehyde and pushing the reaction equilibrium forward to achieve a 100% conversion in 12 h. The C=N bond in *N*-benzylideneaniline was completely cut to obtain high yields of aniline and benzonitrile. As will be discussed later in the Mechanism Study, there exists a reaction equilibrium between

the *N*-phenylethanimine intermediate and aniline/acetaldehyde (Figure 6, 6, 8, and 12), and the presence of $\text{NH}_3\cdot\text{H}_2\text{O}$ pushed this equilibrium forward by constantly consuming the product (acetaldehyde) to form acetonitrile (Figure 6, 12–14), which was detected by GC–MS (Figure S7). The $\text{NH}_3\cdot\text{H}_2\text{O}$ amount showed a weak influence from 100 μL (0.7 mmol) to 400 μL (2.8 mmol) on this transformation. *N*-Ethylaniline conversion increased slowly with increasing $\text{NH}_3\cdot\text{H}_2\text{O}$ amount, while aniline selectivity remained (Table S6). The oxidative cleavage of C–N bonds in *N*-ethylaniline was sensitive to the reaction temperature (Table S7). The conversion greatly increased with an increase in the reaction temperature from 120 to 150 $^\circ\text{C}$, while the aniline selectivity was not influenced by the reaction temperature. After 12 h, aniline was produced in a high selectivity of 95% at the *N*-ethylaniline conversion of 97% at 150 $^\circ\text{C}$ and 10 bar O_2 (Table S8).

Oxidative Cleavage of C–N Bonds in *N*-Alkylanilines and *N,N*-Dialkylanilines into Anilines

The scope of the developed method for the oxidative cleavage of C–N bonds in *N*-alkylanilines and *N,N*-dialkylanilines into anilines was studied. As shown in Figure 4, the different kinds of *N*-alkylanilines (S1–S16) and *N,N*-dialkylanilines (S17–S20) all worked well, affording the desired anilines with good yields. Regarding the *N*-alkylanilines, the activity of these substrates was greatly affected by the electronic properties of the substituted groups. Substrates with electron-withdrawing groups (S2–S7) were much less active than those with electron-donating groups (S8 and S9). Particularly, S7 with the strong electron-withdrawing nitro group proceeded sluggishly at 160 $^\circ\text{C}$, requiring 30 h to get the *p*-nitroaniline product in a yield of 90%, while S8 and S9 with electron-donating substituted groups only need a short reaction time of 4 h at 150 $^\circ\text{C}$ to get the high conversions. In the meanwhile, the electron-donating groups promoted the further oxidative self-coupling of the as-formed anilines to generate azo-compounds,³⁴ which was the reason of the lower product yields from S8 and S9. In addition, the activity of these substrates was also affected by the steric hindrance of the substituted groups. The activity of 4-chloro-*N*-methylaniline (S3), 3-chloro-*N*-methylaniline (S4), and 2-chloro-*N*-methylaniline (S5) greatly decreased in the order of S3, S4, and S5 due to the gradual increase in their steric hindrance. In the meanwhile, S4 and S5 produced the corresponding products with >99% selectivity as the formation of the azo-compounds byproducts was inhibited by the steric hindrance. Furthermore, steric hindrance of the alkyl groups in *N*-alkylanilines also affects the activity of these substrates. Substrates with large steric hindrance (S12 and S13) were much less active than those with small steric hindrance (S10 and S11) since the steric hindrance prevents the dehydrogenation of the H atom from $-\text{C}_\alpha-\text{H}$. In the meanwhile, 1,2-dianilinoethane (S14) with two aniline groups can obtain double yields of aniline. In addition, S15 and S16 with the *N*-benzyl groups were much more active than those with *N*-alkyl groups as the H atom in $-\text{C}_\alpha-\text{H}$ from benzyl groups was much more active than that from alkyl groups.

Besides *N*-alkylanilines, $\text{ZnN}_4\text{-SAC}$ was also effective for the successive cleavage of two C–N bonds in *N,N*-dialkylanilines (S17–S20) into anilines with good yields, while the currently reported catalytic systems could only promote the oxidative cleavage C–N bonds in one alkyl groups in *N,N*-dialkylanilines

to produce *N*-alkylanilines.³⁵ More importantly, this catalytic system can also be extended to the oxidative cleavage of C–N bonds in these challenging substrates with a heterocyclic ring (S21) and *N*-substituted phthalimide (S22), which are very useful in the synthesis of bioactive molecules.

Oxidative Cleavage of C–N Bonds in *N*-Alkylbenzylamines and *N,N*-Dialkylbenzylamines

The oxidative cleavage of C–N bonds in *N*-alkylbenzylamines and *N,N*-dialkylbenzylamines is a challenging issue as the active “ $-\text{CH}_2-$ ” unit in the benzyl group can be readily oxidized into the carbonyl group to generate the stable benzamides.¹⁵ To our great pleasure, the $\text{ZnN}_4\text{-SAC}$ catalyst was also robust for the oxidative cleavage of C–N bonds in *N*-alkylbenzylamines and *N,N*-dialkylbenzylamines, but these products were benzonitriles (Figure 5, S23–S36) not benzylamines. In contrast to the *N*-alkylanilines, the electronic properties of the substituted groups in *N*-alkylbenzylamines (S24 vs S25, S26, and S27) showed no significant influence on the activity. The products from *N*-alkylbenzylamines and *N,N*-dialkylbenzylamines were benzonitrile derivatives, which were formed from the ammoxidation of in situ formed benzaldehyde derivatives. These results suggested that oxidative cleavage of C–N bonds in *N*-alkylbenzylamines started from the oxidation of active “ $\alpha-\text{CH}_2-$ ” in the benzyl fragments not the inactive “ $\alpha-\text{CH}_2-$ ” in the *N*-alkyl groups, where the activation of active “ $\alpha-\text{CH}_2-$ ” in the benzyl fragments was not affected by the electronic properties of the substituted groups in aromatic rings. In the meanwhile, no steric hindrance of the alkyl groups was also observed for these *N*-alkylbenzylamines and *N,N*-dialkylbenzylamines (S28–S36). More interestingly, it was noted that the ammoxidation of benzaldehydes could be performed at room temperature over the $\text{ZnN}_4\text{-SAC}$ catalyst (Figure S8). Thus, our developed catalyst was also effective for the mild and selective ammoxidation of aldehydes into nitriles (Figure S8, S54–S81).

According to the above discussion, the oxidative cleavage of C–N bonds in dibenzylamine (S32) should initially produce benzaldehyde and benzylamine, and the double yields of benzonitrile suggested that benzylamine without *N*-alkyl groups could also be oxidized into benzonitrile. Therefore, the oxidation of benzylamine derivatives into benzonitrile derivatives was also studied. As shown in Figure 5, structurally diverse benzylamine derivatives (S37–S46) were successfully oxidized into benzonitrile derivatives with yields in 85–95% at 120 $^\circ\text{C}$. Besides the synthesis of benzonitrile derivatives, other kinds of nitriles including hetero-aromatic (S47 and S48) and aliphatic (S49–S51) nitriles were also successfully produced from the oxidation of the corresponding primary amines, which are valuable precursors and intermediates for active life science products. Interestingly, the $\text{ZnN}_4\text{-SAC}$ catalyst was also effective for the oxidative cleavage of C–N bonds in α -disubstituted methylamines (S52 and S53) to generate the corresponding ketones. Regarding the oxidative transformation of primary amines into nitriles, the presence of $\text{NH}_3\cdot\text{H}_2\text{O}$ was also very important for the formation of nitriles. The oxidation of benzylamine without $\text{NH}_3\cdot\text{H}_2\text{O}$ produced the corresponding secondary imine as the major product by GC–MS (Figure S9). It is assumed that the oxidative dehydrogenation of benzylamine initially generate the imine intermediate ($\text{C}_6\text{H}_5\text{CH}=\text{NH}$), which then undergoes the coupling reaction with benzylamine to give a secondary imine product by the elimination of one ammonia molecule.³⁶ However, the

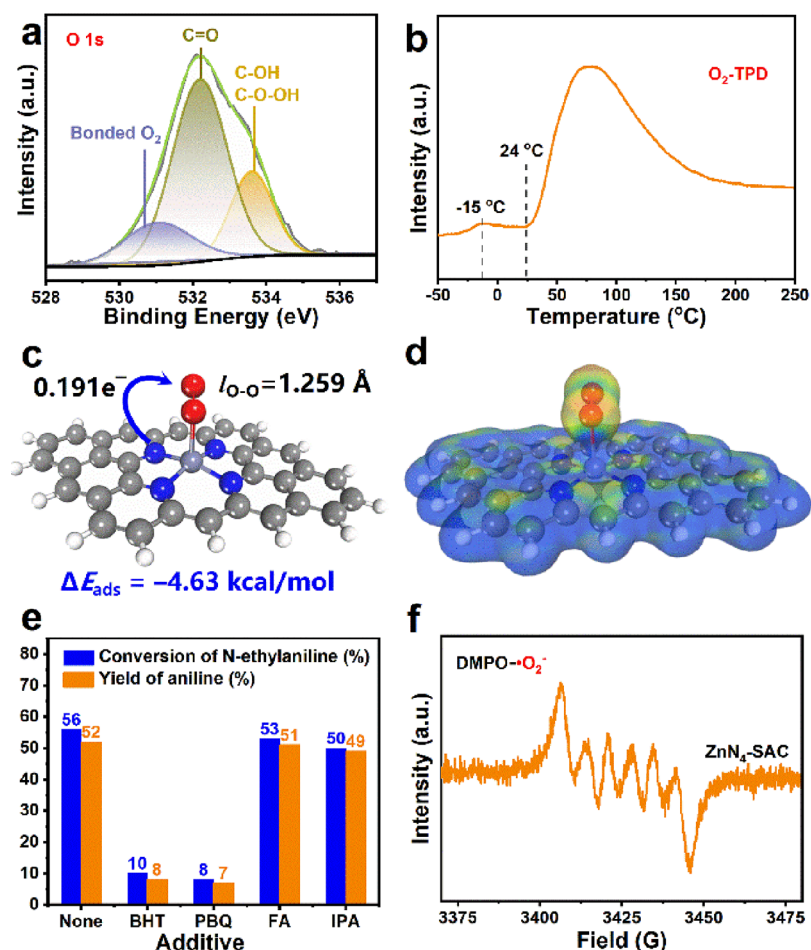


Figure 6. Characterizations of the $\text{ZnN}_4\text{-SAC}$ catalyst for oxygen. (a) O 1s XPS. (b) $\text{O}_2\text{-TPD}$ profiles. (c) Structure of O_2 adsorption and activation over $\text{ZnN}_4\text{-SAC}$. (d) Projected electron density of $\text{ZnN}_4\text{-SAC}$. (e) Radical inhibition experiments of the oxidative transformation of *N*-ethylaniline into aniline. (f) DMPO spin-trapping EPR spectrum of air with $\text{ZnN}_4\text{-SAC}$ in methanol.

presence of $\text{NH}_3\cdot\text{H}_2\text{O}$ can prevent the coupling reaction between the imine intermediate and the benzylamine and promote the further dehydrogenation of the imine intermediate to give a benzonitrile product.

Mechanism Study

As listed in Figure S8, the $\text{ZnN}_4\text{-SAC}$ catalyst could catalyze the ammoxidation of aldehydes into nitriles at room temperature, which suggested that the $\text{ZnN}_4\text{-SAC}$ catalyst should have a strong ability to adsorb and activate O_2 molecules. First, the O 1s XPS spectra of $\text{ZnN}_4\text{-SAC}$ were deconvoluted into three peaks with binding energies at 533.6, 532.2, and 531.1 eV (Figure 6a). The peak at 533.6 eV was assigned to the C–OH and C–O–OH groups, and the peak at 532.2 eV was attributed to the C=O groups. The C–OH/C–O–OH groups and C=O groups are produced by a lignin alkali precursor under the pyrolysis process. The large peak at 531.1 eV was assigned to the adsorbed O_2 molecules during the exposure of $\text{ZnN}_4\text{-SAC}$ in the air,^{30,37,38} suggesting that $\text{ZnN}_4\text{-SAC}$ had a strong ability to adsorb O_2 at room temperature. Due to the instability of Zn–O bonds at 1000 °C³⁹ and the presence of adsorbed O_2 , the O 1s XPS spectra should be derived from the axially coordinated O_2 molecules. O_2 temperature-programmed desorption ($\text{O}_2\text{-TPD}$) profiles of the $\text{ZnN}_4\text{-SAC}$ catalyst also showed a strong desorption peak of O_2 starting at room temperature (Figure 6b), further confirming that the single Zn atoms had strong affinity to O_2 at

low temperatures. Regarding the coordination of O_2 molecules, one model is the side-on coordination model, in which the two oxygen atoms in one O_2 molecule were simultaneously coordinated to the single Zn atom. The other model is the end-on configuration, where only one oxygen atom in the O_2 molecule was coordinated with the Zn– N_4 plane. DFT calculation revealed that the side-on coordination model was not stable, and it can be transformed very fast into the end-on configuration with the adsorption energy in -4.63 kcal/mol (Figure 6c). DFT calculation also revealed that O_2 could be activated by the electron transfer from an electron-rich nitrogen atom to O_2 via single Zn atoms (Figure 6c,d). After the activation, the bond length of O–O increased from 1.208 to 1.259 Å.

Furthermore, the reactive oxygen species were explored during the oxidative transformation of *N*-ethylaniline into aniline over the $\text{ZnN}_4\text{-SAC}$ catalyst by radical inhibition experiments (Figure 6e and Table S9).^{30,40} The conversion greatly decreased from 56% under the standard conditions to 10% in the presence of a radical scavenger of 2,6-di-*tert*-butyl-4-methylphenol (BHT), suggesting that the reaction should proceed via the radical reaction process. The presence of superoxide radical (O_2^-) scavengers (PBQ; 1,4-benzoquinone) greatly inhibited the reaction, while the addition of singlet oxygen ($^1\text{O}_2$) scavengers (FA; furfuryl alcohol) and hydroxyl radical ($\cdot\text{OH}$) scavengers (IPA; iso-propyl alcohol)

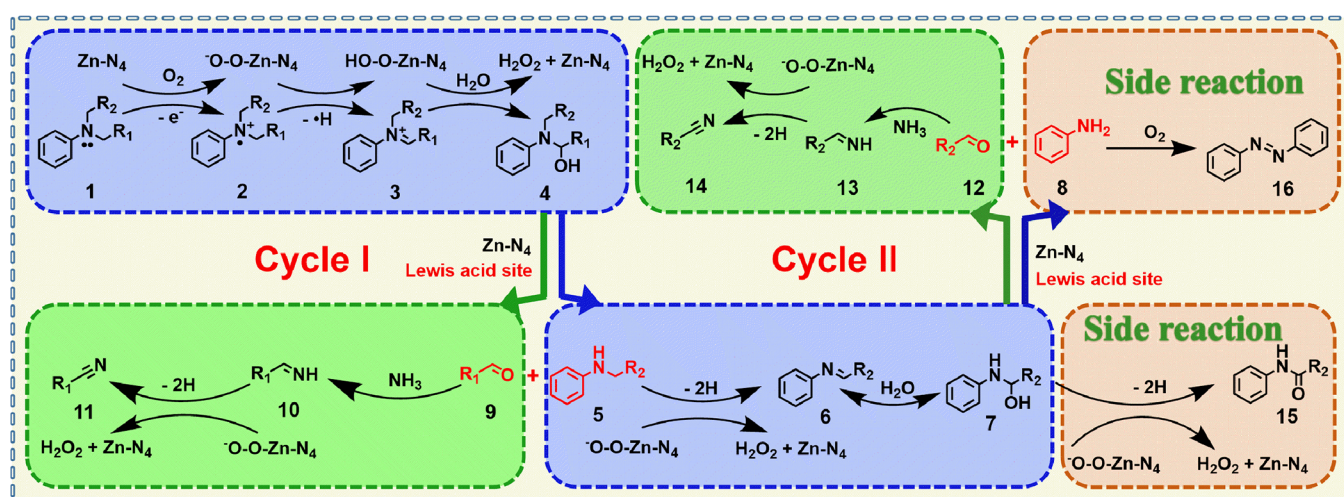


Figure 7. Plausible reaction routes for the oxidative cleavage of C–N bonds in *N,N*-dialkylanilines into *N*-alkylanilines.

showed no significant influence. These controlled experiments confirmed that $\cdot\text{O}_2^-$ was the reactive oxygen species for the oxidative reactions. Next, we used the electron paramagnetic resonance (EPR) technique with 5,5-dimethyl-1-pyrroline *N*-oxide (DMPO) as the spin trap at room temperature. As depicted in Figure 6f, the EPR signal displayed the characteristic fingerprint of spin adducts as a result of $\cdot\text{O}_2^-$, further confirming that the reactive oxygen species was $\cdot\text{O}_2^-$.^{40,41}

After the identification of the reactive oxygen species, the plausible mechanism of oxidative cleavage of C–N bonds in *N*-alkylanilines and *N,N*-dialkylanilines was studied by GC–MS. First, the oxidative transformation of *N*-benzyl-*N*-ethylaniline was performed at 150 °C and 10 bar O_2 (Figure S10a). After 4 h, *N*-ethylaniline as one kind of mono-dealkylation product of *N*-benzyl-*N*-ethylaniline was observed as the major product with a trace amount of *N*-phenylbenzylamine as the other kind of mono-dealkylation product. These results suggested that the $-\text{Csp}^3-\text{H}$ in the benzyl group was more active than the $-\text{Csp}^3-\text{H}$ in the ethyl group, in good accordance with their structure. Aniline as the second C–N bond cleavage product of *N*-phenylbenzylamine or *N*-ethylaniline was also observed. No intermediates were observed for the transformation of *N*-benzyl-*N*-ethylaniline into *N*-phenylbenzylamine or *N*-ethylaniline. *N*-Benzylideneaniline as the intermediate of *N*-phenylbenzylamine into aniline was observed in a very low content, while the intermediate for the oxidative cleavage of *N*-ethylaniline into aniline was not observed. In addition, acetonitrile and benzonitrile from the ammoxidation of the C–N bond cleavage products (acetaldehyde and benzaldehyde) were also formed (Figure S10a).

To capture the intermediates, the reaction time was prolonged to 8 h at 160 °C for the oxidative transformation of *N*-benzyl-*N*-ethylaniline with a high conversion (Figure S10b). The intermediates for the mono-dealkylation of *N*-benzyl-*N*-ethylaniline into *N*-phenylbenzylamine or *N*-ethylaniline were still not observed. In this case, the *N*-benzylideneaniline intermediate of the oxidative transformation of *N*-phenylbenzylamine into aniline was clearly visible, and the *N*-phenylethanamine intermediate of the oxidative cleavage of *N*-ethylaniline into aniline was observed in a trace amount. These results indicated that *N*-benzylideneaniline was much more stable than *N*-phenylethanamine as the C=N bond in *N*-benzylideneaniline can be stabilized by the aromatic

ring, while that was not the case for *N*-phenylethanamine. In addition, some side products such as azobenzene, *N*-phenylbenzamide, and *N*-phenylacetamide were also identified (Figure S10b).

Based on the above analysis, the reaction routes of the oxidative cleavage of C–N bonds in *N,N*-dialkylanilines and *N*-alkylanilines are depicted in Figure 7. According to a reference,¹⁸ the oxidative cleavage of C–N bonds in *N,N*-dialkylanilines can proceed via two possible reaction routes. One route initiates the electron transfer to afford an amine radical cation (2), where the released electron can transfer to the catalyst surface and be used for the activation of O_2 to generate $\cdot\text{O}_2^-$ for the following reactions. After the release of a H radical ($\cdot\text{H}$) from the more active $-\alpha-\text{Csp}^3-\text{H}$ in one alkyl group in tertiary amines, the imine cation intermediates (3) is yielded followed by the addition of one water molecule to generate the α -hydroxylamine intermediates (4). Then, the internal transfer of the H atom from the hydroxyl group to the nitrogen atom in α -hydroxylamine intermediates generates *N*-alkylanilines (5) as the mono-dealkylated product of *N,N*-dialkylanilines and release one aldehyde molecule (9).

According to the above experiment, the oxidative cleavage of C–N bonds in *N*-alkylanilines starts the oxidative dehydrogenation of the two H atoms from $-\text{N}-\text{H}$ and $-\alpha-\text{Csp}^3-\text{H}$ in *N*-alkylanilines by $\cdot\text{O}_2^-$ to generate the imine intermediates (6) and H_2O_2 (Figure S11). Then, the addition of one water molecule to the C=N bond in the imine intermediates generates α -hydroxylamine intermediates (7). Then, the α -hydroxylamine intermediates decompose into anilines (8) and aldehydes (12) via the internal transfer of the H atom from the hydroxyl group to the nitrogen atom in α -hydroxylamine intermediates. The nitriles (11 and 14) were formed by the ammoxidation of in situ formed aldehydes from the dealkylated fragments in *N,N*-dialkylamines and *N*-alkylamines. During the reaction process, some side products were formed. The azo-aromatic byproducts (16) were formed from the hyperoxidation of two anilines, and the amide byproducts (15) were formed by the oxidation dehydrogenation of the two H atoms of $-\text{CH}-\text{OH}$ in α -hydroxylamine intermediates into carbonyl groups.

DFT calculations were then carried out to provide more insights into the reaction mechanism. The oxidative cleavage of *N*-ethylaniline into aniline was used as the model reaction. As

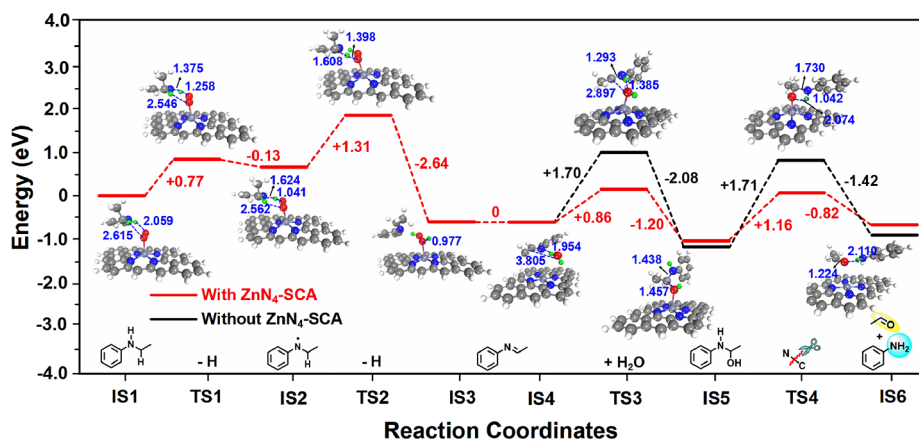
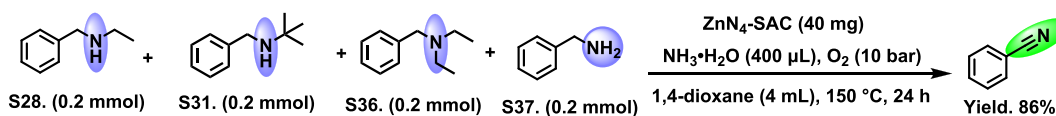
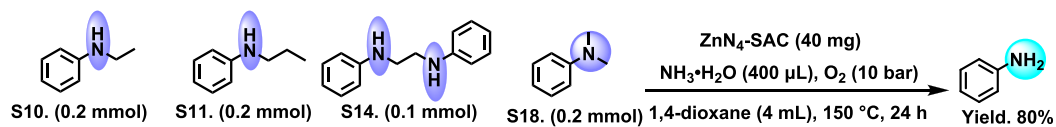
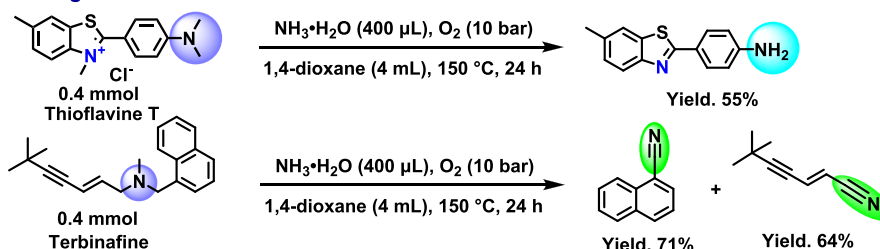


Figure 8. DFT calculation of the oxidative cleavage of *N*-ethylaniline into aniline.

a The C–N bond cleavage of mixed amines in a one-pot reaction



b The cleavage of C–N bond in bioactive molecules



c Gram-scale recycling experiments

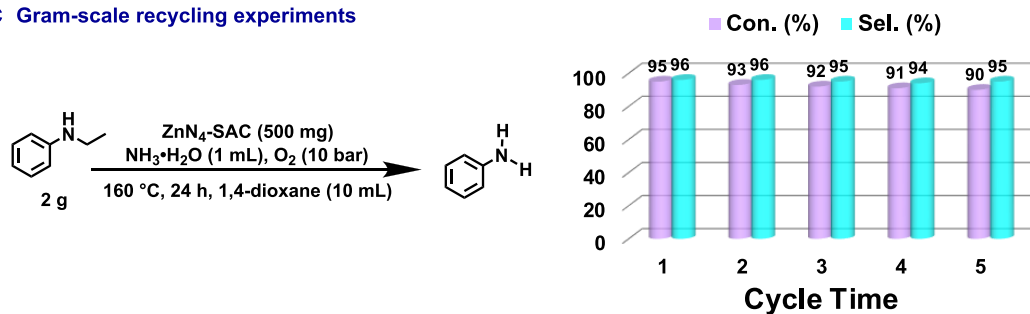


Figure 9. Practical applications of the $\text{ZnN}_4\text{-SAC}$ catalyst. (a) Synthesis of a single product from mixed substrates. (b) Functionalization of bioactive molecules. (c) Recycling experiments in a gram scale.

depicted in Figure 8, *N*-phenylethanamine was the important intermediate, which was formed by the oxidative dehydrogenation of two H atoms from $-\text{N}-\text{H}$ and $-\alpha-\text{Csp}^3-\text{H}$ by $\cdot\text{O}_2^-$. Since the distance between H atoms from $-\text{N}-\text{H}$ and $\cdot\text{O}_2^-$ is smaller than the distance between H atoms from $-\alpha-\text{Csp}^3-\text{H}$ and $\cdot\text{O}_2^-$ (2.095 vs 2.615 Å), the dehydrogenation energy barrier of the H atom from $-\text{N}-\text{H}$ was much smaller than the dehydrogenation energy barrier of the H atom from $\alpha-\text{Csp}^3-\text{H}$ (0.77 vs 1.31 eV). After the formation of *N*-phenyl-

ethanamine, the addition of H_2O to the $\text{C}=\text{N}$ bonds in *N*-phenylethanamine gives the α -hydroxylamine intermediate. DFT calculation revealed that the step of the addition of H_2O to the $\text{C}=\text{N}$ bond was an easy step with a low energy barrier of 0.86 eV over the $\text{ZnN}_4\text{-SAC}$ catalyst. Interestingly, the single Zn atom in the catalyst could lower the energy barrier of this step (0.86 vs 1.70 eV). Then, the C–N bond cleavage accompanied by the H transfer from the $-\text{OH}$ group to the nitrogen atom in α -hydroxylamine intermediate gave rise to

the final product of aniline and acetaldehyde. DFT calculation revealed that the energy barrier of this step was 1.16 eV, which ranked second in the whole reaction process. Similarly, the single Zn atom in the catalyst could also promote the cleavage of C–N bonds by lowering the energy barrier from 1.71 to 1.16 eV. The controlled experiments indicated that the cleavage of C=N bonds in the imine intermediate was indeed greatly promoted over the ZnN₄-SAC catalyst after 2 h at 120 °C (conversion: 32% vs 6%, Figure S12). The NH₃-TPD test (Figure S13) shows that Zn in the ZnN₄-SAC catalyst has obvious Lewis acid properties, which can accelerate the hydrolysis of the imine intermediate into aniline and acetaldehyde.

In addition, the amide side products were also formed with trace amounts, which were formed by the oxidative dehydrogenation of two H atoms from –CH–OH in the α -hydroxylamine intermediates. DFT calculation (Figure S14) revealed that the energy barrier of the oxidation of the α -hydroxylamine intermediate into the amide byproduct was high up to 1.44 eV, which suggested that the oxidation of α -hydroxylamine intermediates into amide side products was much more difficult than the C–N bond cleavage.

Applications of the Developed Methods

One of the most important applications of our developed method was to get a single product from a crude mixture in the chemical industry. For example, a mixture of *N*-alkylanilines and *N,N*-dialkylanilines was successfully converted into a single aniline product with a high yield of 80%. More interestingly, a mixture of benzylamine and *N*-alkyl-benzylamine was successfully converted into a single benzonitrile product with a high yield of 86% (Figure 9a). Second, the developed catalytic system can also be applied for the functionalization of bioactive molecules. Bioactive molecules such as thioflavine T and terbinafine worked well over the developed method, affording the corresponding amine and nitriles with high yields (Figure 9b). More importantly, the catalytic activity remained stable after five large-scale cycle experiments (Figure 9c) without the change of the catalyst structure (Figures S15 and S16).

CONCLUSIONS

In conclusion, a previously unknown catalytic method was developed for the oxidative cleavage of C–N bonds in challenging *N*-alkylamines and *N,N*-dialkylamines with O₂ over the single Zn atom catalyst. The ZnN₄-SAC catalyst could effectively activate O₂ molecules to generate the reactive oxygen species of $\cdot\text{O}_2^-$ even at room temperature and the oxidative dehydrogenation of two H atoms from N–H and –C _{α} –H in *N*-alkylamines to generate the key imine intermediates (C=H). DFT calculation revealed that this step required the highest energy barrier, which was the rate-determining step for the oxidative cleavage of C–N bonds in *N*-alkylamines. In addition, DFT calculation also revealed that the single Zn atoms also served as the Lewis acid sites to promote and lower the energy barriers of the addition of one H₂O molecule into the C=N bonds in the imine intermediates to generate the α -hydroxylamine intermediates and the following C–N bond cleavage via the H atom transfer process. Compared with the reported methods, our developed method showed some distinct advantages such as facile access to the single Zn atom catalyst with low cost, high stability with gram-scale experiments, wide substrate scope, and high selectivity. Our work paves a way to the use of the single

transition metal catalysts with multiple roles in some challenging organic transformations.

EXPERIMENTAL SECTION

Preparation of the ZnN₄-SAC Catalyst

Lignin alkali (2.0 g) was first dispersed in 250 mL of deionized water under magnetic stirring. Zn(NO₃)₂·6H₂O (2.975 g, 10 mmol) was then added into the lignin alkali dispersion, and the mixture was stirred for 12 h. During this process, the Zn²⁺ cations were coordinated with the nitrogen atoms in lignin alkali to get the Zn–lignin complex. After the washing of free Zn²⁺ from the Zn–lignin complex, it was dried. Then, the as-obtained Zn–lignin complex was mixed with 10 times the weight of dicyandiamide by grinding in a mortar. The composite was heated from room temperature to 550 °C at a rate of 5 °C/min under a nitrogen atmosphere, and it was kept at 550 °C for 1 h. Then, the temperature was increased to 1000 °C at a rate of 5 °C/min, and the sample was annealed at 1000 °C for 1 h. After cooling to room temperature under a N₂ atmosphere, the single atom Zn catalyst was obtained (ZnN₄-SAC).

Preparation of the NC-1000 Catalyst

The NC-1000 catalyst was prepared by direct pyrolysis of the mixture of lignin alkali with 10 times the weight of dicyandiamide.

Preparation of the Zn–N_x/NC-1100 Catalyst

The preparation of Zn–N_x/NC-1100 is the same as that of ZnN₄-SAC except that the calcination temperature was changed to 1100 °C.

Other Experimental Details

Other experimental details are provided in the Methods Section in the Supporting Information.

ASSOCIATED CONTENT

Supporting Information

The Supporting Information is available free of charge at <https://pubs.acs.org/doi/10.1021/jacsau.2c00605>.

Experimental procedure, characterization data, computational details, and NMR spectra (PDF)

AUTHOR INFORMATION

Corresponding Author

Zehui Zhang – School of Chemistry and Materials Science, South-Central Minzu University, Wuhan, Hubei 430074, P. R. China; orcid.org/0000-0003-1711-2191; Email: zehuizh@mail.ustc.edu.cn

Authors

Jingzhong Qin – School of Chemistry and Materials Science, South-Central Minzu University, Wuhan, Hubei 430074, P. R. China

Bo Han – Sustainable Energy Laboratory, Faculty of Materials Science and Chemistry, China University of Geosciences, Wuhan, Hubei 430074, P. R. China

Xiaomei Lu – School of Chemistry and Materials Science, South-Central Minzu University, Wuhan, Hubei 430074, P. R. China

Jiabao Nie – School of Chemistry and Materials Science, South-Central Minzu University, Wuhan, Hubei 430074, P. R. China

Chensheng Xian – School of Chemistry and Materials Science, South-Central Minzu University, Wuhan, Hubei 430074, P. R. China

Complete contact information is available at: <https://pubs.acs.org/10.1021/jacsau.2c00605>

Author Contributions

J.Q. and B.H. contributed equally to this work. J.Q.: conceptualization, data curation, formal analysis, investigation, methodology. B.H.: DFT calculation. X.L.: data curation, formal analysis. J.N.: data curation. C.X.: data curation. Z.Z.: conceptualization, funding acquisition, project administration, supervision, writing (review and editing).

Notes

The authors declare no competing financial interest.

ACKNOWLEDGMENTS

The authors thank the National Natural Science Foundation of China (21922513) for their support.

REFERENCES

- (1) Murugesan, K.; Senthamarai, T.; Chandrashekar, V. G.; Natte, K.; Kamer, P. C. J.; Beller, M.; Jagadeesh, R. V. Catalytic reductive aminations using molecular hydrogen for synthesis of different kinds of amines. *Chem. Soc. Rev.* **2020**, *49*, 6273.
- (2) Dighe, S. U.; Juliá, F.; Luridiana, A.; Douglas, J. J.; Leonori, D. A photochemical dehydrogenative strategy for aniline synthesis. *Nature* **2020**, *584*, 75–81.
- (3) Zhang, B.; Guo, T.; Liu, Y.; Kühn, F. E.; Wang, C.; Zhao, Z. K.; Xiao, J.; Li, C.; Zhang, T. Sustainable production of benzylamines from lignin. *Angew. Chem., Int. Ed.* **2021**, *60*, 20666–20671.
- (4) Gandomkar, S.; Fischereder, E.-M.; Schrittwieser, J. H.; Wallner, S.; Habibi, Z.; Macheroux, P.; Kroutil, W. Enantioselective oxidative aerobic dealkylation of N-ethyl benzyloquinolines by employing the berberine bridge enzyme. *Angew. Chem., Int. Ed.* **2015**, *54*, 15051–15054.
- (5) Wu, J.; Li, L.; Liu, M.; Bai, L.; Luan, X. Selective C(sp³)–N bond cleavage of N, N-dialkyl tertiary amines with the loss of a large alkyl group via an SN₁ pathway. *Angew. Chem., Int. Ed.* **2021**, *60*, No. e2021138.
- (6) Denisov, I. G.; Makris, T. M.; Sligar, S. G.; Schlichting, I. Structure and chemistry of cytochrome P450. *Chem. Rev.* **2005**, *105*, 2253–2278.
- (7) Bhakta, M. N.; Wimalasena, K. A mechanistic comparison between cytochrome P450- and chloroperoxidase-catalyzed N-dealkylation of N, N-dialkyl anilines. *Eur. J. Org. Chem.* **2005**, 4801–4805.
- (8) Basran, J.; Patel, S.; Sutcliffe, M. J.; Scrutton, N. S. Importance of barrier shape in enzyme-catalyzed reactions. *J. Biol. Chem.* **2001**, *276*, 6234–6242.
- (9) Najmi, A. A.; Jafariyeh-Yazdi, E.; Hadian, M.; Hermans, J.; Bischoff, R.; Yue, J.; Dömling, A.; Wittstock, A.; Permentier, H. P. Nanoporous gold catalyst for the oxidative N-dealkylation of drug molecules: A method for synthesis of N-dealkylated metabolites. *ChemMedChem* **2022**, *17*, No. e2022000.
- (10) Kim, S.; Ginsbach, J. W.; Lee, J. Y.; Peterson, R. L.; Liu, J. J.; Siegler, M. A.; Sarjeant, A. A.; Solomon, E. I.; Karlin, K. D. Amine oxidative N-dealkylation via cupric hydroperoxide Cu–OOH homolytic cleavage followed by site-specific fenton chemistry. *J. Am. Chem. Soc.* **2015**, *137*, 2867–2874.
- (11) Xiang, J.; Peng, M.; Pan, Y.; Luo, L.-J.; Cheng, S.-C.; Jin, X.-X.; Yiu, S.-M.; Man, W.-L.; Ko, C.-C.; Lau, K.-C.; Lau, T.-C. Visible light-induced oxidative N-dealkylation of alkylamines by a luminescent osmium(VI) nitrido complex. *Chem. Sci.* **2021**, *12*, 14494.
- (12) Limnios, D.; Kokotos, C. G. 2,2,2-trifluoroacetophenone as an organocatalyst for the oxidation of tertiary amines and azines to N-oxides. *Chem. – Eur. J.* **2014**, *20*, 559–563.
- (13) Jin, X.; Kataoka, K.; Yatabe, T.; Yamaguchi, K.; Mizuno, N. Supported gold nanoparticles for efficient α-oxygenation of secondary and tertiary amines into amides. *Angew. Chem., Int. Ed.* **2016**, *55*, 7212–7217.
- (14) Klobukowski, E. R.; Mueller, M. L.; Angelici, R. J.; Woo, L. K. Conversions of cyclic amines to nylol precursor lactams using bulk gold and fumed silica catalysts. *ACS Catal.* **2011**, *1*, 703–708.
- (15) Kim, J. W.; Yamaguchi, K.; Mizuno, N. Heterogeneously catalyzed efficient oxygenation of primary amines to amides by a supported ruthenium hydroxide catalyst. *Angew. Chem., Int. Ed.* **2008**, *47*, 9249–9251.
- (16) Lu, Y. J.; Zhang, X.; Malakar, S.; Krogh-Jespersen, K.; Hasanayn, F.; Goldman, A. S. Formation of enamines via catalytic dehydrogenation by pincer-iridium complexes. *J. Org. Chem.* **2020**, *85*, 3020–3028.
- (17) Ling, Z.; Yun, L.; Liu, L. H.; Wu, B.; Fu, X. Aerobic oxidative N-dealkylation of tertiary amines in aqueous solution catalyzed by rhodium porphyrins. *Chem. Commun.* **2013**, *49*, 4214.
- (18) Zhao, H.; Leonori, D. Minimization of back-electron transfer enables the elusive sp³ C–H functionalization of secondary anilines. *Angew. Chem., Int. Ed.* **2021**, *60*, 7669–7674.
- (19) Yang, X.-F.; Wang, A.; Qiao, B.; Li, J.; Liu, J.; Zhang, T. Single-atom catalysts: a new frontier in heterogeneous catalysis. *Acc. Chem. Res.* **2013**, *46*, 1740–1748.
- (20) Jones, J.; Xiong, H.; DeLaRiva, A. T.; Peterson, E. J.; Pham, H.; Challa, S. R.; Qi, G.; Oh, S.; Wiebenga, M. H.; Hernández, X. I. P.; Wang, Y.; Datsy, A. K. Thermally stable single-atom platinum-on-ceria catalysts via atom trapping. *Science* **2016**, *353*, 150–154.
- (21) Lang, R.; Du, X.; Huang, Y.; Jiang, X.; Zhang, Q.; Guo, Y.; Liu, K.; Qiao, B.; Wang, A.; Zhang, T. Single-atom catalysts based on the metal-oxide interaction. *Chem. Rev.* **2020**, *120*, 11986–12043.
- (22) Zou, X.-P.; Wang, L.-N.; Li, X.-N.; Liu, Q.-Y.; Zhao, Y.-X.; Ma, T.-M.; He, S.-G. Noble-metal-free single-atom catalysts CuAl₄O₇–9[–] for CO oxidation by O₂. *Angew. Chem., Int. Ed.* **2018**, *57*, 10989–10993.
- (23) Luo, L.; Luo, J.; Li, H.; Ren, F.; Zhang, Y.; Liu, A.; Li, W.-X.; Zeng, J. Water enables mild oxidation of methane to methanol on gold single-atom catalysts. *Nat. Commun.* **2021**, *12*, 1218.
- (24) Li, T.; Liu, F.; Tang, Y.; Li, L.; Miao, S.; Su, Y.; Zhang, J.; Huang, J.; Sun, H.; Haruta, M.; Wang, A. Q.; Qiao, B.; Li, J.; Zhang, T. Maximizing the number of interfacial sites in single-atom catalysts for the highly selective, solvent-free oxidation of primary alcohols. *Angew. Chem., Int. Ed.* **2018**, *57*, 7795–7799.
- (25) Yang, Q.; Yang, C.-C.; Lin, C.-H.; Jiang, H.-L. Metal–organic-framework-derived hollow N-doped porous carbon with ultrahigh concentrations of single Zn atoms for efficient carbon dioxide conversion. *Angew. Chem., Int. Ed.* **2019**, *58*, 3511–3515.
- (26) Zhu, Y.; Sun, W.; Chen, W.; Cao, T.; Xiong, Y.; Luo, J.; Dong, J.; Zheng, L.; Zhang, J.; Wang, X. L.; Chen, C.; Peng, Q.; Wang, D.; Li, Y. Scale-up biomass pathway to cobalt single-site catalysts anchored on N-doped porous carbon nanobelt with ultrahigh surface area. *Adv. Funct. Mater.* **2018**, *28*, No. 1802167.
- (27) Bai, L.; Hsu, C.-S.; Alexander, D. T. L.; Chen, H. M.; Hu, X. A cobalt–iron double-atom catalyst for the oxygen evolution reaction. *J. Am. Chem. Soc.* **2019**, *141*, 14190–14199.
- (28) Yang, F.; Song, P.; Liu, X.; Mei, B.; Xing, W.; Jiang, Z.; Gu, L.; Xu, W. Highly efficient CO₂ electroreduction on ZnN₄-based single-atom catalyst. *Angew. Chem., Int. Ed.* **2018**, *57*, 12303–12307.
- (29) Lin, Y.; Liu, P.; Velasco, E.; Yao, G.; Tian, Z.; Zhang, L.; Chen, L. Fabricating single-atom catalysts from chelating metal in open frameworks. *Adv. Mater.* **2019**, *31*, No. 1808193.
- (30) Xie, C.; Lin, L.; Huang, L.; Wang, Z.; Jiang, Z.; Zhang, Z.; Han, B. Zn–N_x sites on N-doped carbon for aerobic oxidative cleavage and esterification of C(CO)–C bonds. *Nat. Commun.* **2021**, *12*, 4823.
- (31) Liu, W.; Zhang, L.; Liu, X.; Liu, X.; Yang, X.; Miao, S.; Wang, W.; Wang, A.; Zhang, T. Discriminating catalytically active FeN_x species of atomically dispersed Fe–N–C catalyst for selective oxidation of the C–H bond. *J. Am. Chem. Soc.* **2017**, *139*, 10790–10798.
- (32) Zhang, L.; Bi, X.; Guan, X.; Li, X.; Liu, Q.; Barry, B.-D.; Liao, P. Chemoselective oxidative C(CO)–C(methyl) bond cleavage of methyl ketones to aldehydes catalyzed by CuI with molecular oxygen. *Angew. Chem., Int. Ed.* **2013**, *52*, 11303–11307.

(33) Tang, C.; Jiao, N. Copper-catalyzed aerobic oxidative C–C bond cleavage for C–N bond formation: from ketones to amides. *Angew. Chem., Int. Ed.* **2014**, *53*, 6528–6532.

(34) Dutta, B.; Biswas, S.; Sharma, V.; Savage, N. O.; Alpay, S. P.; Suib, S. L. Mesoporous manganese oxide catalyzed aerobic oxidative coupling of anilines to aromatic azo compounds. *Angew. Chem., Int. Ed.* **2016**, *55*, 2171–2175.

(35) Cybularczyk-Cecotka, M.; Predyger, J.; Crespi, S.; Szczepanik, J.; Giedyk, M. Photocatalysis in aqueous micellar media enables divergent C–H arylation and N-dealkylation of benzamides. *ACS Catal.* **2022**, *12*, 3543–3549.

(36) Ma, Z.; Liu, S.; Tang, N.; Song, T.; Motokura, K.; Shen, Z.; Yang, Y. Coexistence of Fe nanoclusters boosting Fe single atoms to generate singlet oxygen for efficient aerobic oxidation of primary amines to imines. *ACS Catal.* **2022**, *12*, 5595–5604.

(37) Shang, S.; Chen, P.-P.; Wang, L.; Lv, Y.; Li, W.-X.; Gao, S. Metal-free nitrogen- and boron-codoped mesoporous carbons for primary amides synthesis from primary alcohols via direct oxidative dehydrogenation. *ACS Catal.* **2018**, *8*, 9936–9944.

(38) Datsyuk, V.; Kalyva, M.; Papagelis, K.; Parthenios, J.; Tasis, D.; Siokou, A.; Kallitsis, I.; Galiotis, C. Chemical oxidation of multiwalled carbon nanotubes. *Carbon* **2008**, *46*, 833–840.

(39) Pan, Y.; Chen, Y.; Wu, K.; Chen, Z.; Liu, S.; Cao, X.; Cheong, W.-C.; Meng, T.; Luo, J.; Zheng, L.; Liu, C.; Wang, D.; Peng, Q.; Li, J.; Chen, C. Regulating the coordination structure of single atom Fe–N_xC_y catalytic sites for benzene oxidation. *Nat. Commun.* **2019**, *10*, 4290.

(40) Qin, J.; Han, B.; Liu, X.; Dai, W.; Wang, Y.; Luo, H.; Lu, X.; Nie, J.; Xian, C.; Zhang, Z. An enzyme-mimic single Fe–N₃ atom catalyst for the oxidative synthesis of nitriles via C–C bond cleavage strategy. *Sci. Adv.* **2022**, *8*, No. eadd1267.

(41) Zhao, X.; Wang, F.; Kong, X.-P.; Fang, R.; Li, Y. Dual-metal hetero-single-atoms with different coordination for efficient synergistic catalysis. *J. Am. Chem. Soc.* **2021**, *143*, 16068–16077.